Deformation Along the San Andreas Fault South of the Coseismic and Postseismic October 18, 1989, Loma Prieta M_L 7.1 Earthquake Rupture

By Robert J. Mueller[1] and M. J. S. Johnston[1]

Open-File Report 00-146

2000

U.S. DEPARTMENT OF THE INTERIOR
U.S. GEOLOGICAL SURVEY

[1]Menlo Park, California

Table of Contents

Abstract. Deformation along a 14 km segment of the San Andreas fault (SAF), from near the southern end of the October 18, 1989 Loma Prieta earthquake rupture to San Juan Bautista has been measured with a nine-site trilateration network since 1981. Model calculations obtained from inversion of the large-scale geodetic and strong-motion data from the Loma Prieta earthquake do not fit the data obtained from this geodetic network. To fit the observed coseismic displacements, additional oblique coseismic slip of 57 cm is required on a 8 km by 3 km seismically active fault segment on the SAF beneath the northern part of the network together with 86 cm of strike-slip motion on a 10 km by 4 km segment on the Sargent fault. This suggests that the southern extent of the Loma Prieta rupture extended at least 10-15 km further to the southeast than previously thought and involved sympathetic slip on the Sargent fault. Continuing postseismic displacements were observed in these data between December, 1989 and October, 1990. During this period the largest Loma Prieta aftershock (Chittenden earthquake M_L5.4), and a major aftershock sequence, occurred beneath the geodetic network in April, 1990. Future data will show if postseismic slip rates on the San Andreas fault within the Pajaro network after 1990 have increased compared to the well determined 7mm/yr before the earthquake. We suspect this will be so since two adjacent segments of the fault beneath the southern part of the network have failed largely aseismically in the form of slow earthquakes in 1992 and 1996 and independent surface creep and continuous strain rates are higher after the earthquake than before.

Introduction

A network of intermediate baseline geodetic benchmarks (Figure 1) was installed in 1981 in expectation that an earthquake might rupture the San Andreas fault (SAF) through the southern Santa Cruz mountains to San Juan Bautista. The Loma Prieta earthquake (October 18, 1989; M_L=7.1) occurred on a previously unrecognized segment of the SAF with an epicenter some 35 km to the northwest of the network center. Inversion of data obtained from benchmark displacements (Figure 1) throughout the region (*Lisowski et al.*, 1990; *Marshall et al.*, 1991; *Snay et al.*, 1991; *Williams et al.*, 1993; *Arnadottir and Segall*, 1994) indicates that most of the data, particularly at the north, east and west sites, can be explained by rupture of a 30 to 37 km long segment of the San Andreas fault from 8 to 18 km deep with oblique slip ranging from 5.5 m to 1.5 m as the fault geometry increases from its minimum to maximum values. Even better fits were obtained with

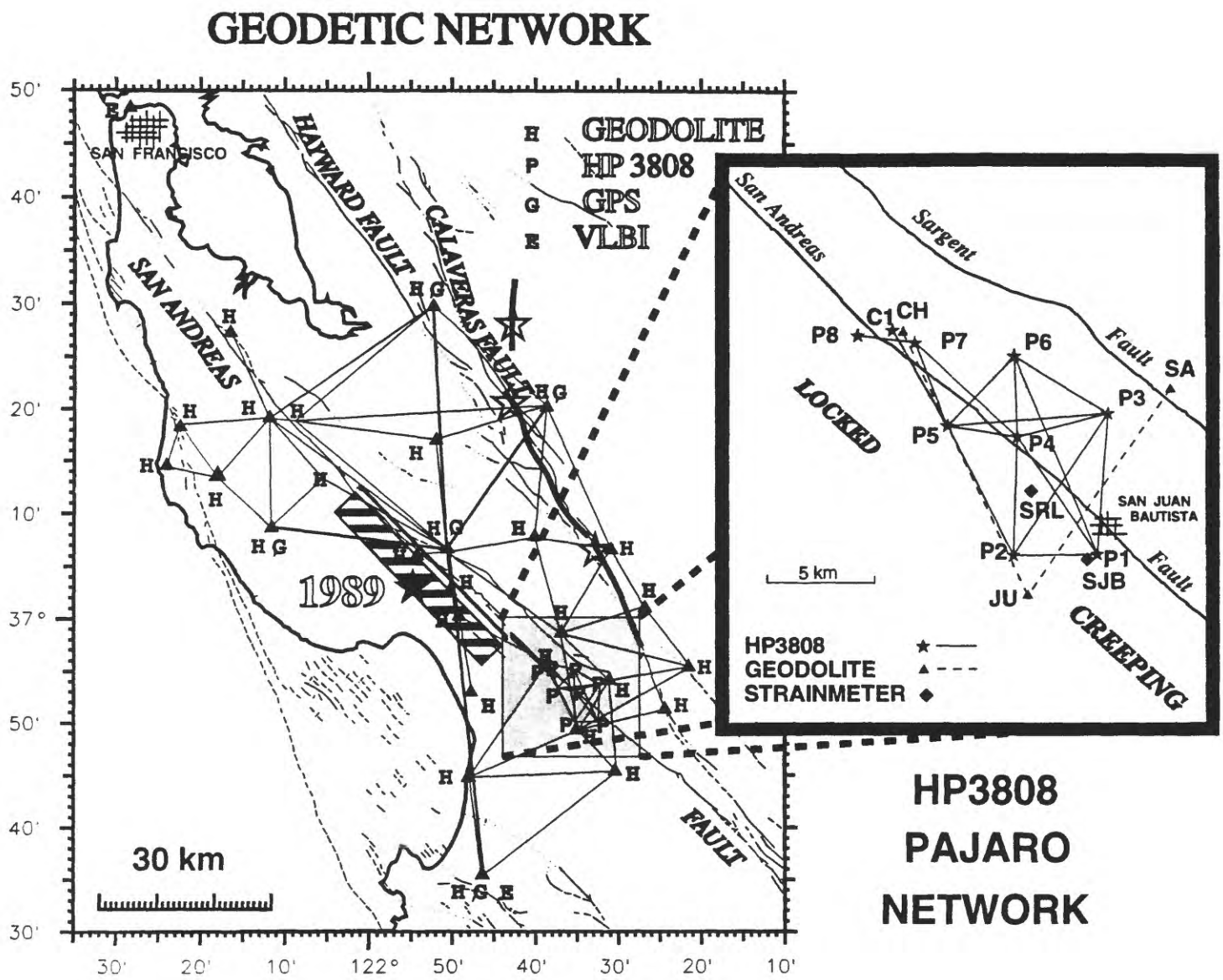

Figure 1. Map of the San Andreas fault system from San Francisco to Central California showing faults, geodetic sites, and recent moderate earthquakes (stars). The location of the Pajaro EDM network is shown shaded and inset near the southern end of the Loma Prieta rupture (shaded rectangle). The epicenter of the Loma Prieta earthquake is shown with a solid star.

non-uniform slip models (*Beroza*, 1991; *Hartzell et al.*, 1991; *Steidl et al.*, 1991; *Wald et al.*, 1991; *Arnadottir and Segall*, 1994; *Horton*, 1996). The details of the various uniform slip models are listed in Table 1. The poor fits of these single slip patch models to the few geodetic and GPS data near the southern end of the rupture indicate problems with these models (*Lisowski et al.*, 1990). The few published data are not sufficient to determine the detailed geometry of the rupture here and the role the Sargent fault might have played in this earthquake even though intense aftershock activity extended at least 15 km along the SAF from the southern end of the modeled rupture and on the Sargent fault (*Dietz and Ellsworth*, 1990). Surface displacements were also observed on the Sargent fault (*Aydin et al.*, 1992; *Marshall et al.*, 1991).

The data reported here also are too few to provide a full understanding of what occurred here but they do provide some useful hints. In particular, they support the suggestion that the Loma Prieta rupture extended into the Pajaro region although the slip was much less than that during the main shock and may have been triggered by the main shock. Furthermore, shallow, possibly triggered, slip probably occurred on the Sargent fault. Most importantly, inclusion of Loma Prieta slip in the Pajaro region is consistent with the strain offsets measured independently on borehole strainmeters in the region (*Johnston et al.*, 1990; *Gwyther et al.*, 1992).

The data also suggest that significant postseismic slip occurred on the San Andreas fault in this region during 1990 and may have triggered, or been triggered by, the April 18, 1990, Chittenden M_L 5.4 earthquake - the largest aftershock of the Loma Prieta earthquake. Post-seismic slip is also suggested by increased rates of surface creep within, and to the southeast of the network, from 1990 to 1992 (*Behr et al.*, 1997) and increased strain rates recorded on nearby borehole strainmeters following both the mainshock and the aftershock (*Johnston et al.*, 1990; *Gwyther et al.*, 1992). Most significantly, sections of the SAF beneath the network failed largely aseismically in 1992 (*Linde et al.*, 1996) and in 1996 (*Johnston et al.*, 1997).

To illustrate this sequence of events, we first isolate coseismic and postseismic displacements generated local to the network by removing the secular displacement rates in the region (*Gu and Prescott*, 1986) and the coseismic displacements generated by the main Loma Prieta rupture (*Lisowski et al.*, 1990; *Marshall et al.*, 1991; *Snay et al.*, 1991; *Williams et al.*, 1993; *Arnadottir and Segall*, 1994). The coseismic and postseismic residuals are then best-fit with simple uniform-slip elastic-dislocation models to determine the main features of slip in the region during and following the Loma Prieta earthquake.

Table 1. Fault Parameters for Uniform Slip Models

STUDY		STRIKE (degrees)	DIP	TOP km	WIDTH km	LENGTH km	STRIKE-SLIP m	DIP-SLIP m	MOMENT 10^{19} MPa
Lisowski et al., 1990		N44W	70	5	12.3	37	1.66	1.19	3.0
Marshall et al., 1991		N52W	60	4	9	34	2.38	1.66	2.7
Snay et al., 1991	(upper)	N45.6W	90	4.8	4.2	32.4	1.86	1.06	0.9
	(lower)	same	70	9.0	6.1	same	1.96	2.3	1.8
Williams et al., 1993		N50W	70	4.5	11	31	1.8	2.3	3.0
Arnadottir & Segall, 1994		N47.6W	75.8	7.6	4.6	30.3	5.2	4.6	2.9

The Pajaro Network

The Pajaro network (Figure 1 - insert) is uniquely located over a 14 km long segment of the SAF that covers the transition between the section of the fault that is continuously creeping (i.e. to the SE of the network) into the section that had been previously locked (i.e. to the NW of the network). Line lengths within the Pajaro geodetic network are measured using a Hewlett Packard model 3808 (HP3808) electronic distance measuring device (EDM). The measurement precision is about 1.5 ppm and the standard deviation (mm) as a function of line-length is given by,

$$\sigma=[(a)^2+(b*X)^2]^{1/2}$$

where a and b are equal to 3 mm and 1.0 mm/km, respectively, and X is the line-length measurement in kilometers (*Lisowski and Prescott*, 1981). The precision of line-length measurements in the network range from 4 mm to 15 mm. Measurements are made using a tripod mounted HP3808 and retro-reflectors centered above permanent benchmarks. End point meteorology measurements (air temperature, atmospheric pressure, and humidity) are used to correct for changes in the refractive index of the air along the travel path. Shaded measurements of these meteorological parameters were made at both the instrument and reflector sites and averaged to estimate the refractive index along the path. Temperature measurements were made at a 5 m height with digital thermometers accurate to 0.4°C.

Line lengths are measured in both directions and the corrected mean distance is weighted by the standard deviation of the measurements and used with the site elevation and tripod height differences to calculate the mark to mark distances and sea level distances described by *Bomford* (1971). For the analysis described here, the distances used are all sea level distances and any lines greater than 7 km in length are not used in this study because repeatability could not be demonstrated. Individual line-lengths are shown in Appendix A and benchmark locations and azimuths are given in Appendix B.

Distances for lines JU-CH and JU-SA (Figure 1) are measured with a "Geodolite" EDM. Aircraft measurements of atmospheric temperature and humidity and ground measurements of pressure are use to correct the refractive index. The precision obtained with this technique is about 0.2 ppm (*Savage and Prescott*, 1973).

To test the quality of our EDM data, we compared data from the EDM lines P5-C1 and P5-P7 with that from the Geodolite line JU-CH (Figure 1) These lines are different in length (P5-C1 is 5.5 km. P5-P7 is 4.1 km, and JU-CH is 13.4 km) but they have the same general azimuth and cross the

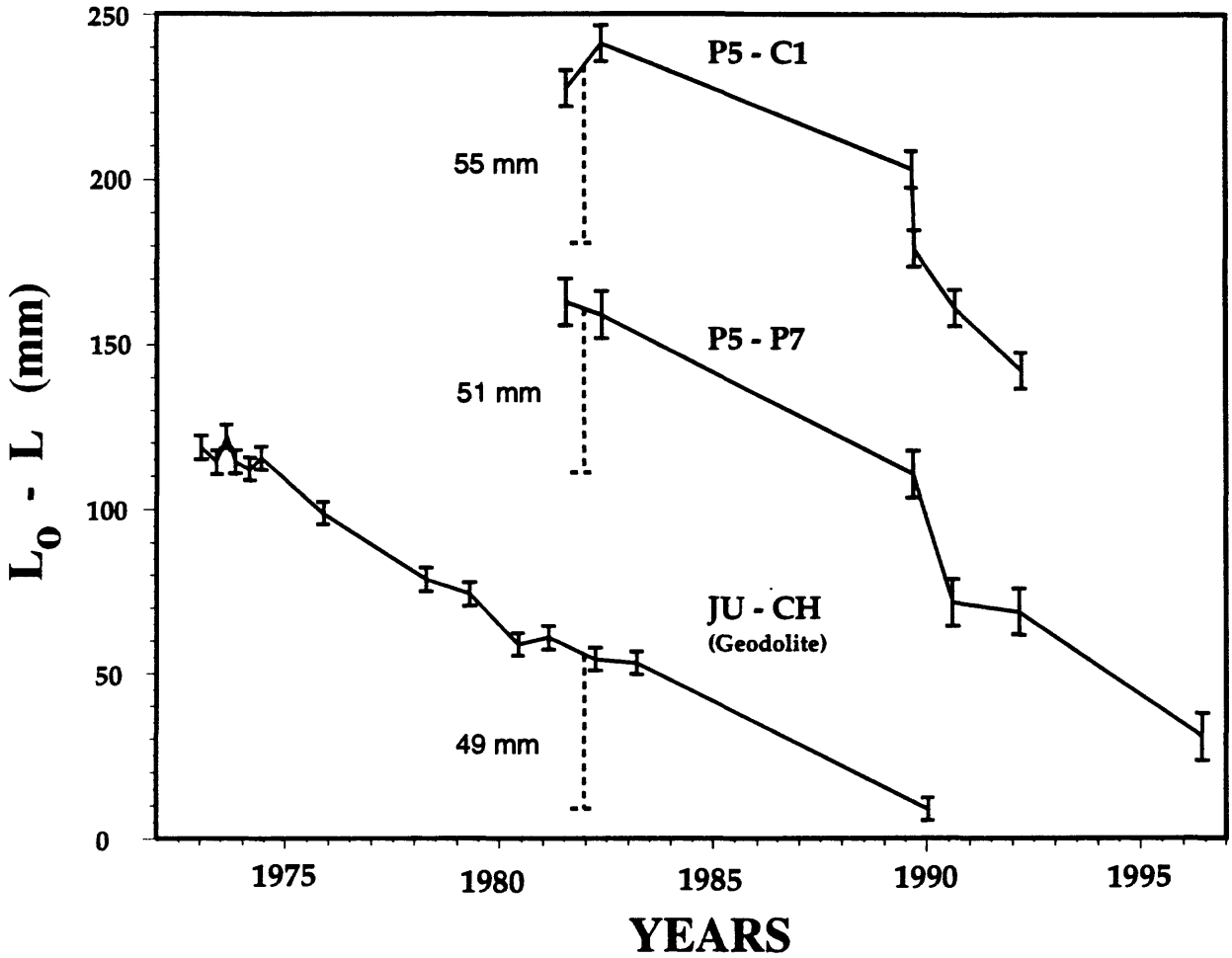

Figure 2. Comparison of HP3808 EDM distance measurements for the line P5-C1 and P5-P7 with the geodetically measured line JU-CH for the period 1972 to 1996. Changes between 1982 and 1990 are shown by vertical dashed lines.

SAF within a 0.7 km section. Figure 2 shows a comparison of the data from these lines which indicates that, between 1982 and 1990, the two independent measurement systems recorded similar displacements (49mm, 51 mm and 55 mm) of which only a few mm was due to the Loma Prieta main rupture (as calculated using the *Arnadottir and Segall* (1994) model). Thus, the majority of the observed displacement appears due to right-lateral block-like slip motion on the SAF, since measurements on all three lines show similar total displacements but the EDM lines P5-C1 and P5-P7 are less than half the length of the JU-CH line. This should come as no surprise since *Gu and Prescott* (1986) used all available Geodolite EDM data in the region from 1972-1983 to show that the primary characteristic behavior of the San Andreas fault in this region from Pajaro gap (PG) to a point 10 km south of San Juan Bautista (SJB) was block slip of 8.8 mm/yr with a further 14.5 mm/yr of block slip occurring on the Calaveras fault. Furthermore, the slip direction on the San Andreas is more parallel to the Calaveras than to the San Andreas fault. Since the total plate slip in this region is 33 mm/yr, the remaining 10 mm/yr must be distributed through the region or on other minor faults such as the San Gregorio, Zayante, Vergales, Sargent, Ortigalita, etc.

Since the fault south of San Juan Bautista (where most of the Geodolite lines are located) is creeping while that in the north (i.e. the SJB-PG region discussed in this paper) is not, *Gu and Prescott*'s (1986) value of 8.8 mm/yr is biased high. Indeed, subsets of data in the northern PG region reported by *Lisowski et al.*, (1996) and including the JU-CH line (shown in Figure 2) indicate blockslip from 1973-1990 of 7 mm/yr. Furthermore, observed long-term surface creep near San Juan Bautista (SJB) at the south of this region reported by *Behr et al.*, (1997) indicate the net slip here at the south end is also 7 mm/yr. Thus, a secular rate due to 7 mm/yr of fault slip is imposed on these data and needs to be removed before details of the Loma Prieta earthquake can be investigated.

Seismicity

The seismicity pattern along the San Andreas fault, for the eight year period prior to the Loma Prieta earthquake, indicates the fault was largely aseismic NW of geodetic site P4 (Figure 3, upper left). Seismicity is observed along the San Andreas fault SE of site P4 (*Dietz and Ellsworth*, 1990) and surface fault creep is observed along the fault SE of site P1 (*Behr et al.*, 1997). The previously locked sections on both the SAF and the Sargent fault exhibited strong aftershock activity following the Loma Prieta earthquake, as shown during the first week in Figure 3 (upper right) and

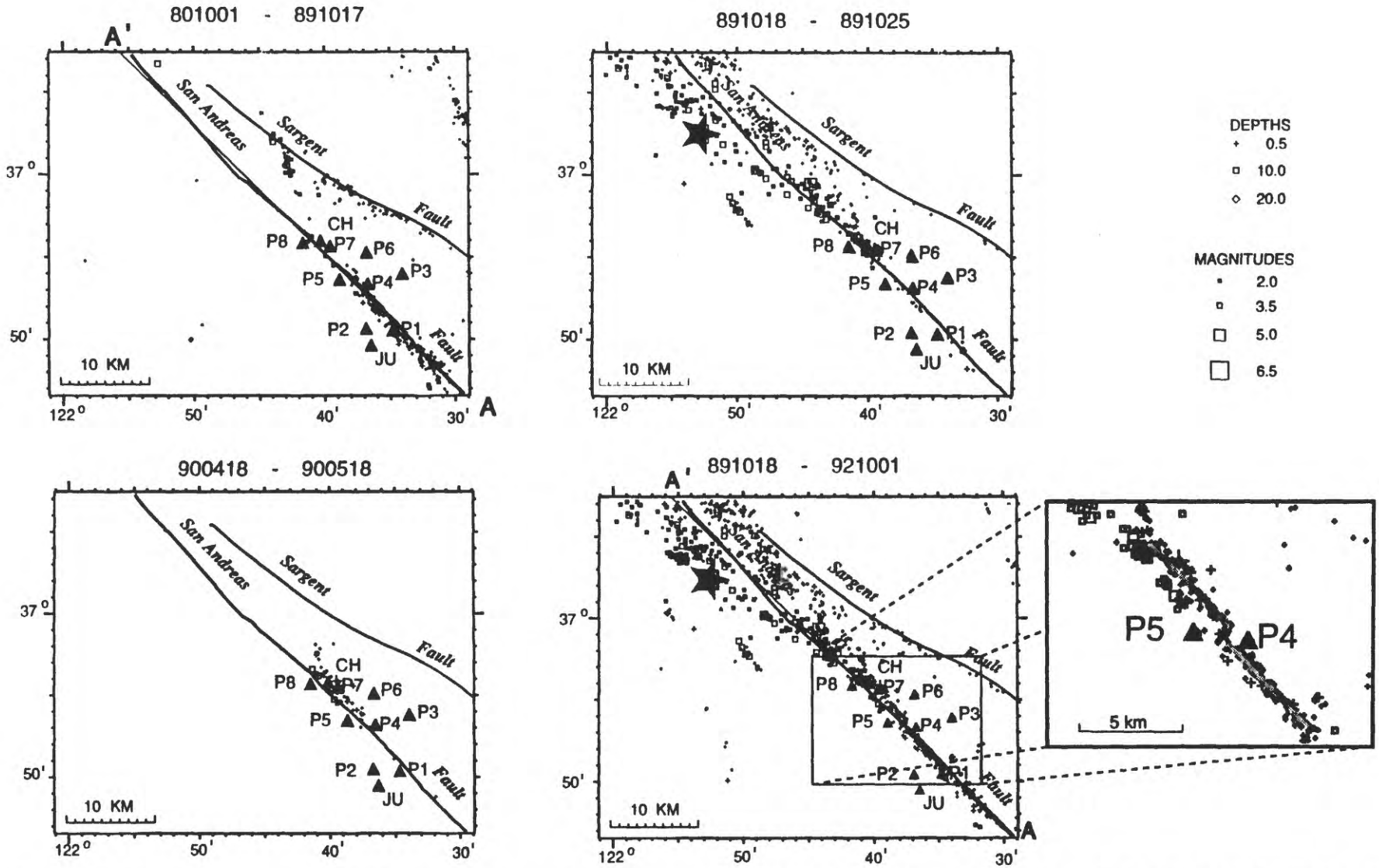

Figure 3. Seismicity maps showing earthquake magnitudes and depths in relation to the Pajaro Network for the periods: 1) October 1, 1980 to October 18, 1989 (Upper Left) prior to the Loma Prieta earthquake, 2) October 18 to October 25, 1989 (Upper Right) immediately after the earthquake, 3) April 18 to May 18, 1990 (Lower Right) covering the Chittenden earthquake, and 4) October 18, 1989 to October 1, 1992 (Lower Center) covering the primary aftershock sequence. The epicenter of the Loma Prieta earthquake is shown as a large star on the Upper Left and Lower Center plots. The inset in the Lower Center plot shows an expanded view of the en echelon or right step in the seismicity between sites P4 and P5. Also shown on the upper left and lower right plot is the line AA' along the San Andreas on which the seismicity is projected in the following cross-section plots.

during the first three years in Figure 3 (lower right). Also shown in Figure 3 (lower left) is the aftershock activity from April 18, 1990 to May 18, following the April 18, 1990 Chittenden aftershock (M_L5.4), the largest event in the Loma Prieta aftershock sequence. This event occurred immediately beneath site P7. Also evident is an apparent but minor offset in seismicity on the SAF between P4 and P5 as shown in the expanded section of Figure 3 (lower right).

The aftershocks near the SAF were projected onto the SAF (line AA' in Figure 3). Figure 4 (upper left) shows the pre-1989 seismicity in cross-section in relation to the Pajaro network and the future aftershock region of the Chittenden earthquake (grey hatching). The transition from the creeping to the locked section of the SAF is located just to the north of site P1 near the southern end of the Pajaro geodetic network (*Wesson et al.*, 1973). The aftershock cross-section for the first week after the earthquake is shown in Figure 4 (top right) and that during the Chittenden aftershock is shown in Figure 4 (lower left). The absence of seismicity in this grey hatched area before and after the Loma Prieta earthquake suggests that this zone did not break during or immediately after the Loma Prieta earthquake. If so, it probably was no surprise that it ruptured as an aftershock in 1990.

The overall aftershock pattern of the Loma Prieta event (Figure 4, bottom right) shows a shallowing of seismicity from north to south from depths of about 20 km to about 10 km. An apparent hole in the aftershock distribution occurs under P1 to P4 to a depth of about 7 km. It is interesting to note that this section failed largely aseismically in a slow earthquake in December, 1992 (*Linde et al.*, 1996) and again in 1996 during aseismic failure of a second section just to the north (*Johnston et al.*, 1997). In general, the majority of aftershocks shown in this cross-section for the first three years after the earthquake occurred in the previously locked section of the fault.

Observed Displacements

The changes in line-length for the individual lines as a function of time between 1981 and 1996 are plotted in Figure 5a and 5b. Following the Loma Prieta earthquake, five surveys were completed in the seven year period from 1989 to 1996 except at site P3. Data were no longer collected at this site after 1990 because the benchmark was destroyed. Also, site P2 was not surveyed in 1996 because of difficulties in getting access to the property on which it is located. Individual line-length measurements are shown in Appendix A.

The most obvious features of the data are:

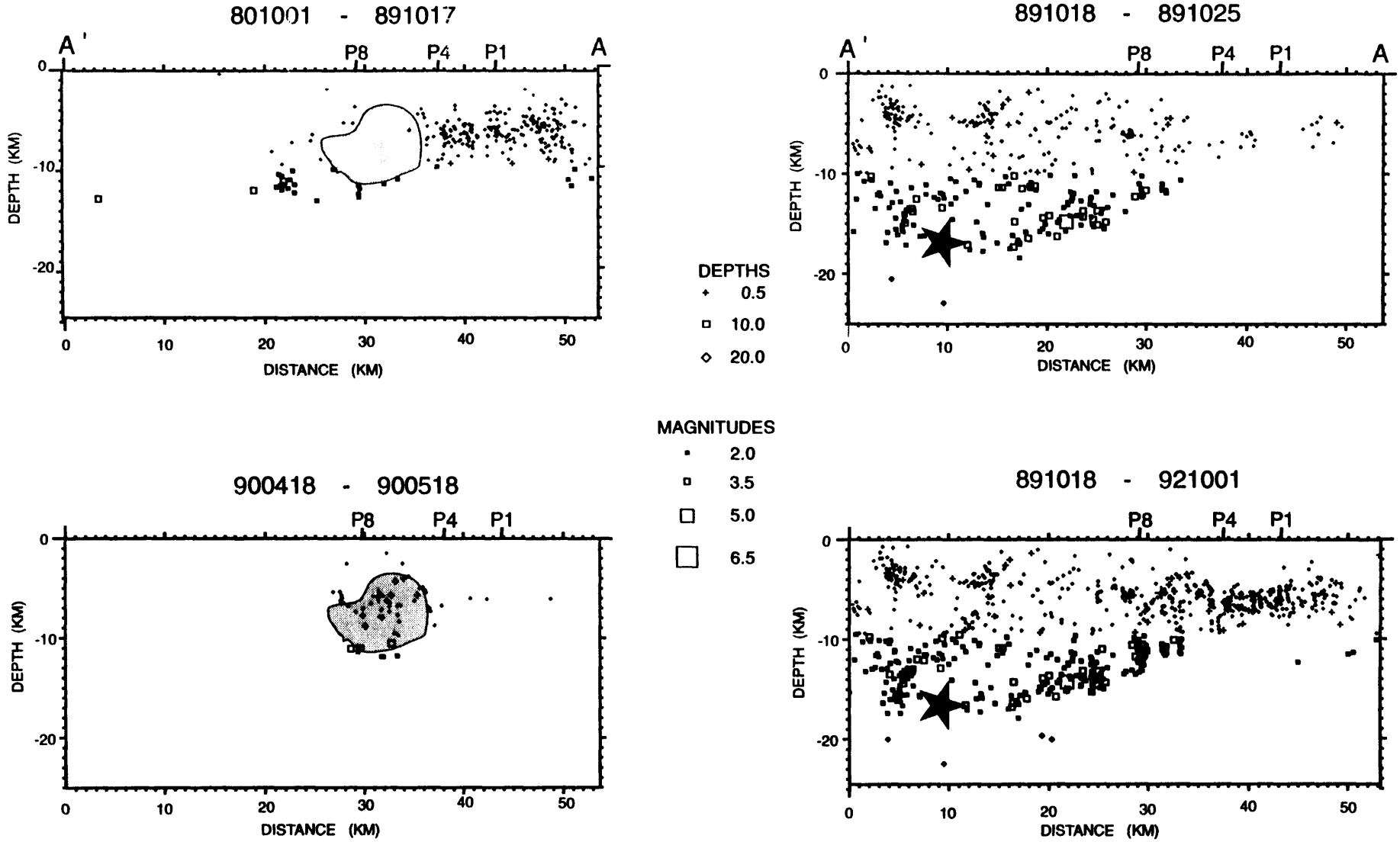

Figure 4. Seismicity cross-sections projected onto the plane of the San Andreas fault beneath AA′ for the time periods: 1) October 1, 1980 to October 18, 1989 (Upper Left) - prior to the Loma Prieta earthquake, 2) October 18 to October 25, 1989 (Upper Right) - the immediate postseismic period, 3) April 18 to May 18, 1990 (Lower Right) - the period round the time of the Chittenden earthquake, and 4) October 18, 1989 to October 1, 1992 (Lower Left) - the primary aftershock period. The two right side plots cover the time of the Loma Prieta earthquake (shown as a star). The Chittenden aftershock sequence (Lower Left) is shown (shaded) on the two left side plots.

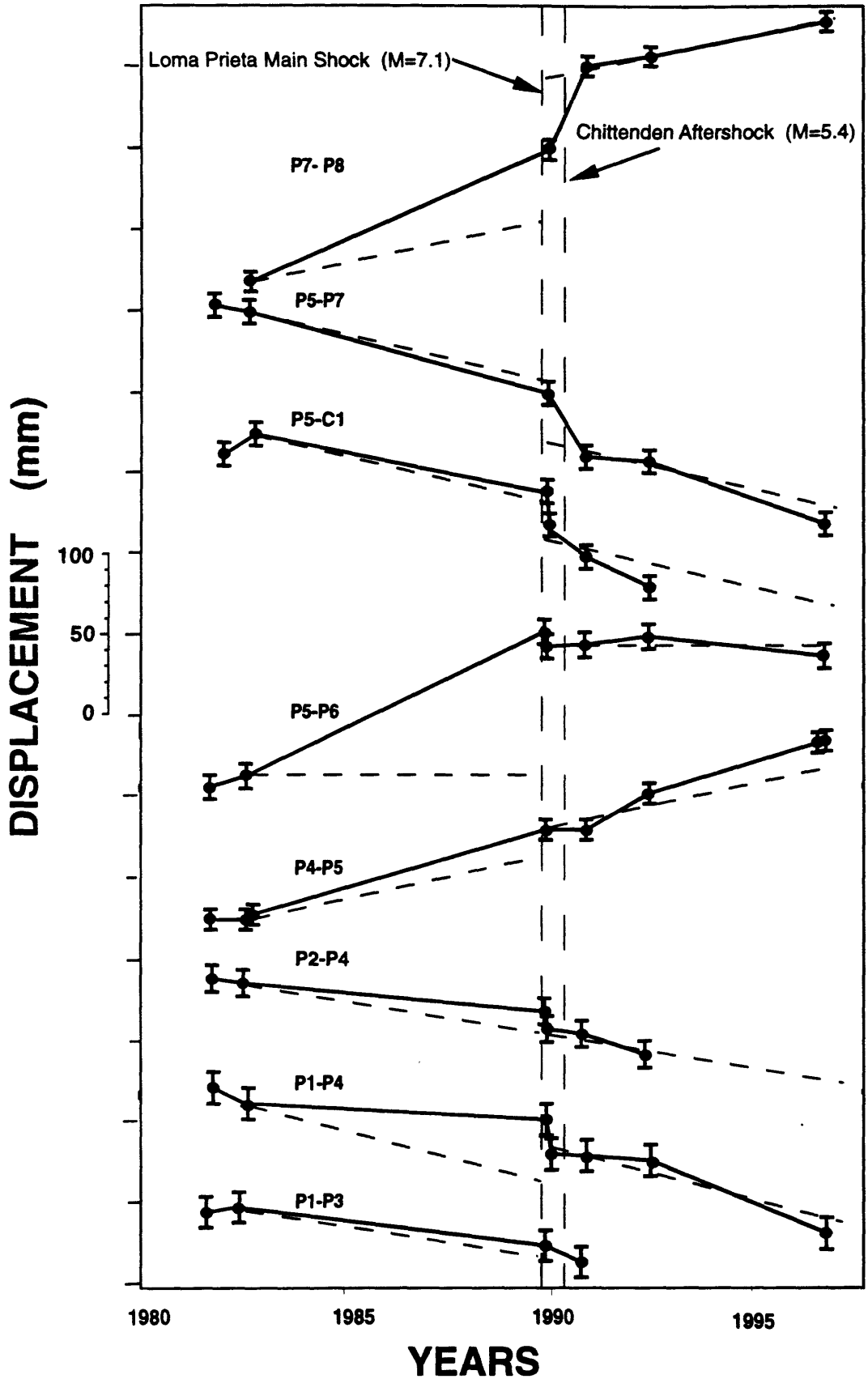

Figure 5a. Line length changes (and error estimates) as a function of time for eight of the Pajaro network lines. The dashed lines show the change in line length expected for each line from the geodetically determined secular strain (7mm/yr) in the region prior to the Loma Prieta earthquake and for the postseismic period. The occurrence times of the Loma Prieta and Chittenden earthquakes are shown as vertical dashed lines.

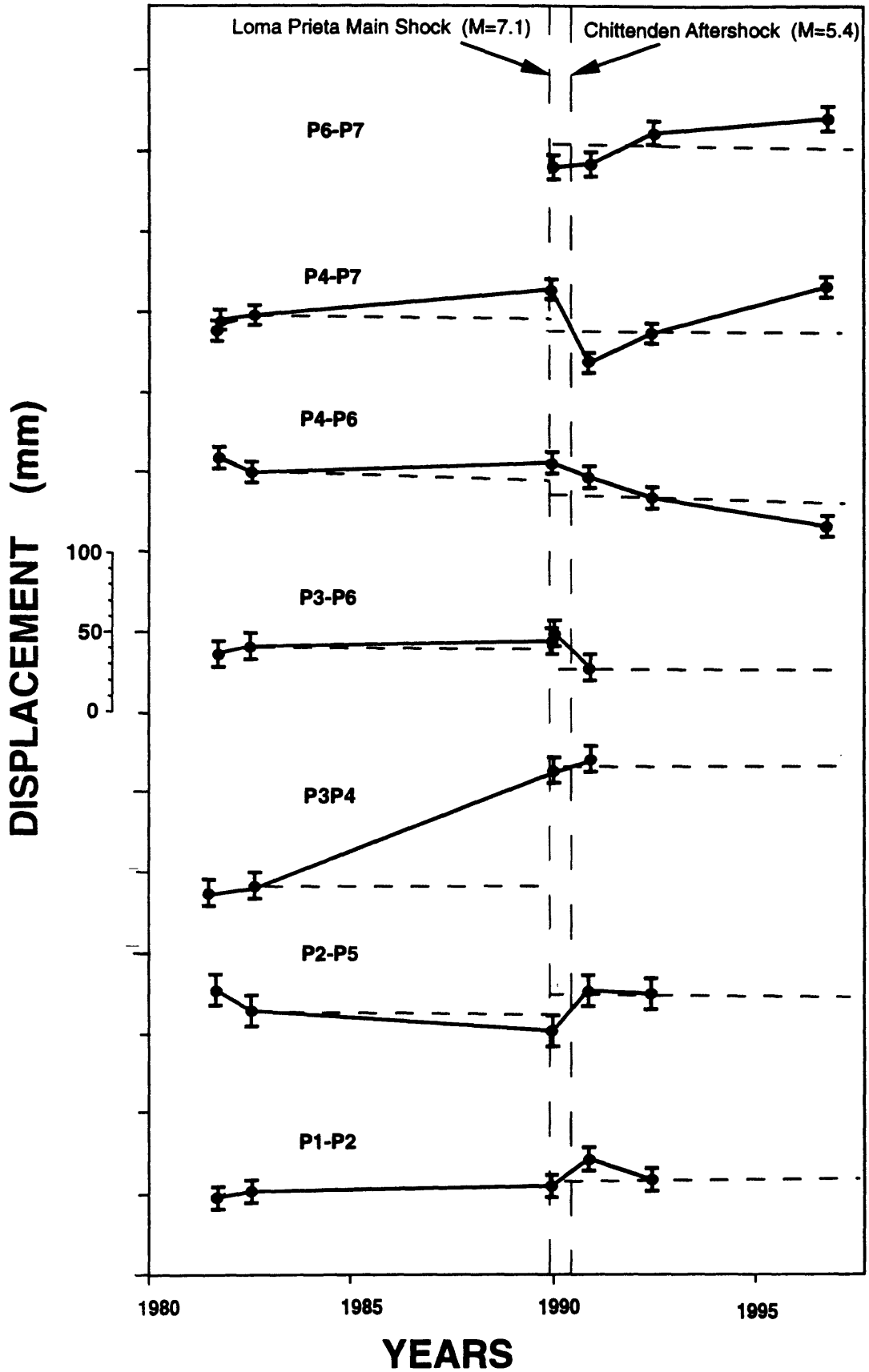

Figure 5b. Line length changes (and error estimates) as a function of time for seven of the Pajaro network lines. The dashed lines show the change in line length expected for each line from the geodetically determined secular strain (7mm/yr) in the region prior to the Loma Prieta earthquake and for the postseismic period. The occurrence times of the Loma Prieta and Chittenden earthquakes are shown as vertical dashed lines.

1) large changes in line-length produced by the earthquake on fault crossing lines closest to the epicenter of the Loma Prieta earthquake and north of site P4 (Figure 5a),

2) substantial postseismic displacements observed on many lines. Best examples of this are seen on P7-P8, P5-P7, P4-P7, and P2-P5 between December, 1989 and November, 1990. Many, but not all, of these changes involve site P7 and most of the changes appear to have occurred after the February 1990 observation of line JU-CH (See Figure 2).

3) suggestions on some lines that rates of line-length change after the earthquake are larger than those before the earthquake,

4) strong extension of the fault-normal and fault-crossing line P5-P6 and the non fault-crossing line P3-P4 produced by the Loma Prieta earthquake. Indications of postseismic contraction occurred in P4-P6 and P1-P2.

5) changes observed both before and after the Loma Prieta earthquake that are much larger than expected from the published models of the earthquake (*Lisowski et al.*, 1990; *Marshall et al.*, 1991; *Snay et al.*, 1991; *Williams et al.*, 1993; *Arnadottir and Segall*, 1994).

6) the overall effect of the Loma Prieta earthquake was to shear and to dilate the northern part of the Pajaro network.

To isolate effects due to the Loma Prieta earthquake, its aftershocks, and other effects, we have removed the secular displacement rates due to block slip of 7 mm/yr (*Gu and Prescott*, 1986; *Behr et al.*, 1997; *Lisowski et al.*, 1996) from the data in the region (as discussed above). We modeled this slip with a simple block displacement model in which 7 mm/yr occurs on a 60 km long and 20 km wide fault beneath the network (*Okada*, 1985) and calculated the expected displacement rates for each line during the period from 1982 to October, 1989. These displacement rates are shown in Figures 5a and 5b as dashed lines. While no data were collected between 1982 and 1989 because of efforts to upgrade the Parkfield region at the other end of the creeping section of the fault, these displacement rates over the region are assumed to be uniform during this time - an assumption that is supported by the continuous and more sensitive strain data in the region (*Johnston et al.*, 1990). The residuals (termed observed coseismic) are listed in Table 2.

The data were also processed using the various analysis techniques discussed in *Welsch* (1979), *Prescott*, (1981) and *Gu and Prescott* (1986) for display of displacement data in strike-slip environments.

Table 2. Summary of Coseismic Displacements (mm).

LINE	Coseismic Observed (OBS)*	Loma Prieta Earthquake Main Shock (AS)	Residual (OBS-AS)	Total Model Model 1 (TM1)	Residual (OBS-TM1)	Model 2 (TM2)	Residual (OBS-TM2)
			FAULT CROSSING				
P7-P8	41 ±5	8	33	41	0	43	- 2
P5-P7	-6±5	- 18	12	- 37	31	- 4	- 2
P5-C1	-7 ±6	- 18	11	- 39	32	- 20	13
P5-P6	84 ±6	- 14	98	62	24	30	54
P4-P5	12 ±5	14	- 2	49	- 37	41	- 29
P2-P4	8 ±6	- 21	29	32	- 24	10	- 2
P1-P4	28 ±7	5	23	32	- 4	24	4
P1-P3	17±7	- 25	42	4	13	14	3
			NONFAULT CROSSING				
P4-P7	16±7	5	11	- 13	29	- 9	- 25
P4-P6	8 ±5	- 20	28	- 42	50	- 20	28
P4-P3	74 ±5	- 5	79	18	- 11	1	73
P3-P6	7 ±6	9	- 2	73	1	0	6
P2-P5	-11 ±7	2	- 13	12	- 23	8	19
P1-P2	9 ±5	12	- 3	11	- 2	10	- 1

* Corrected for 7 mm/a interseismic slip on the San Andreas Fault (1982 - 1989).

Discussion

The large changes in line length and the active seismicity in this region during and following the Loma Prieta earthquake raise immediate suspicions of significant tectonic activity in this region. Unfortunately, understanding this activity is difficult with data from only 12 EDM lines and two continuous strainmeters in the region. The few long-length Geodolite lines are, for most part, too far away to be of much help. Thus, the data are sufficient to deal with only the simplest models of coseismic and postseismic behavior.

As a first step, we initially tried inverting all of the data reported in *Lisowski et al.*, (1990) and strain data from *Johnston et al.*, (1990) using the inversion method of *Marquardt* (1963), as described by *Bevington* (1969), for least squares estimation of coseismic failure on the main Loma Prieta rupture and on the San Andreas fault in the vicinity of the Pajaro network. The starting model was restricted to be on the San Andreas fault and we attempted to solve for slip, with perturbations in width and length. In the inversion procedure, weighting of the various points uses the reciprocal of the error estimates. For the EDM lines we used 2σ listed in Table 2 and in *Lisowski et al.*, (1990). For the strain data we used errors of 20% of the observed signals. We were able to find models for which the Chi-square values (ie misfit squared) could be minimized to less than 8. However, detailed investigation showed the misfits in just the Pajaro region were still poor and that the total data set, mostly involving sites to the north and near the large main Loma Prieta rupture, was not very sensitive to detailed slip in the Pajaro region (no sites there).

To focus on the Pajaro region and to isolate coseismic effects generated by the primary rupture from those perhaps generated more local to the Pajaro network, we next calculated displacements generated from the simplest models of the Loma Prieta earthquake previously obtained by inversion of the large-scale geodetic, and leveling data (*Lisowski et al.*, 1990; *Marshall et al.*, 1991; *Snay et al.*, 1991; *Williams et al.*, 1993; *Arnadottir and Segall*, 1994) then removed these displacements from the observed data in the Pajaro network. These models differ only in the fine details (Table 1) and predict quite similar displacements at each of the benchmarks within the Pajaro network. The best-fit simple models (*Lisowski et al.*, 1990; *Marshall et al.*, 1991; *Snay et al.*, 1991; *Williams et al.*, 1993; *Arnadottir and Segall*, 1994) indicate that most of the large-scale data can be explained by rupture of a 30 to 37 km long segment of the San Andreas fault from 6 to 18 km deep with strike-slip and reverse slip ranging from 5.5 m to 1.5 m for the smallest to largest fault geometries. All of the models underestimate the observed amplitude and sense of motion of the

different benchmarks in the Pajaro network. We chose one of the more recent models (*Arnadottir and Segall*, 1994) as the representative model for the Loma Prieta earthquake since it has the smallest fault geometry. In this model the rupture length is 30 km with 5.2 m of strike-slip and 4.6 m of dip-slip motion.

Displacements at each of the sites were calculated for this primary rupture model (termed AS) using the formulation for an elastic dislocation from *Okada* (1985). These were converted into line-length changes and are listed in Table 2. It is apparent that the observed offsets are not in agreement with the offsets expected at this location from the AS model (or, for that matter, any other model). The model misfit to the Pajaro data is 6.5 mm/mm which is worse than that for a null model (5.6). This problem is even more apparent if we view these data as vector displacements, as discussed above, where we again hold the azimuth of the P1-P4 line and the position of site P1 fixed. The calculated coseismic displacement vectors for the AS model are shown in Figure 6 as dashed arrows. The net coseismic displacement vectors (and associated errors) produced by the Loma Prieta earthquake are shown by the solid line vectors in Figure 6 when the direction of the fault parallel line P1-P4 line and the position of site P1 are held fixed. Again, there is almost no agreement between the model and the observed displacements either in direction or amplitude of the changes. The residual, coseismic displacement vectors obtained by differencing the AS model and observation vectors are large (Figure 7) and a different slip model is obviously required to fit the observed coseismic displacements in the Pajaro region.

We now investigate various models that might explain these observed coseismic data. Because of our limited data, we have restricted our search for slip models to those located on either the San Andreas and Sargent faults, or both, where most of the aftershock activity was located. This simplified our search through model space enormously since we constrain position, length, width, dip, depth and the only unknown parameters are slip. We also looked at small perturbations in length, width and depth of the fault to see how sensitive the solution was to the chosen values. In some cases, we also allowed dip on the San Andreas to vary. We also carried out grid point searches over a generous range of parameters in order to verify the stability of the various parameters even though we are limited by the few data available.

Several best fitting models were obtained with model misfits less than 4.5 mm/mm and others are no doubt possible. The two primary candidates require slip on both the Sargent and the San Andreas faults and, in both cases, the amount of slip required is substantially less than that on the main fault rupture, as expected if this slip were triggered. The best of these (misfit 4.1) is physi-

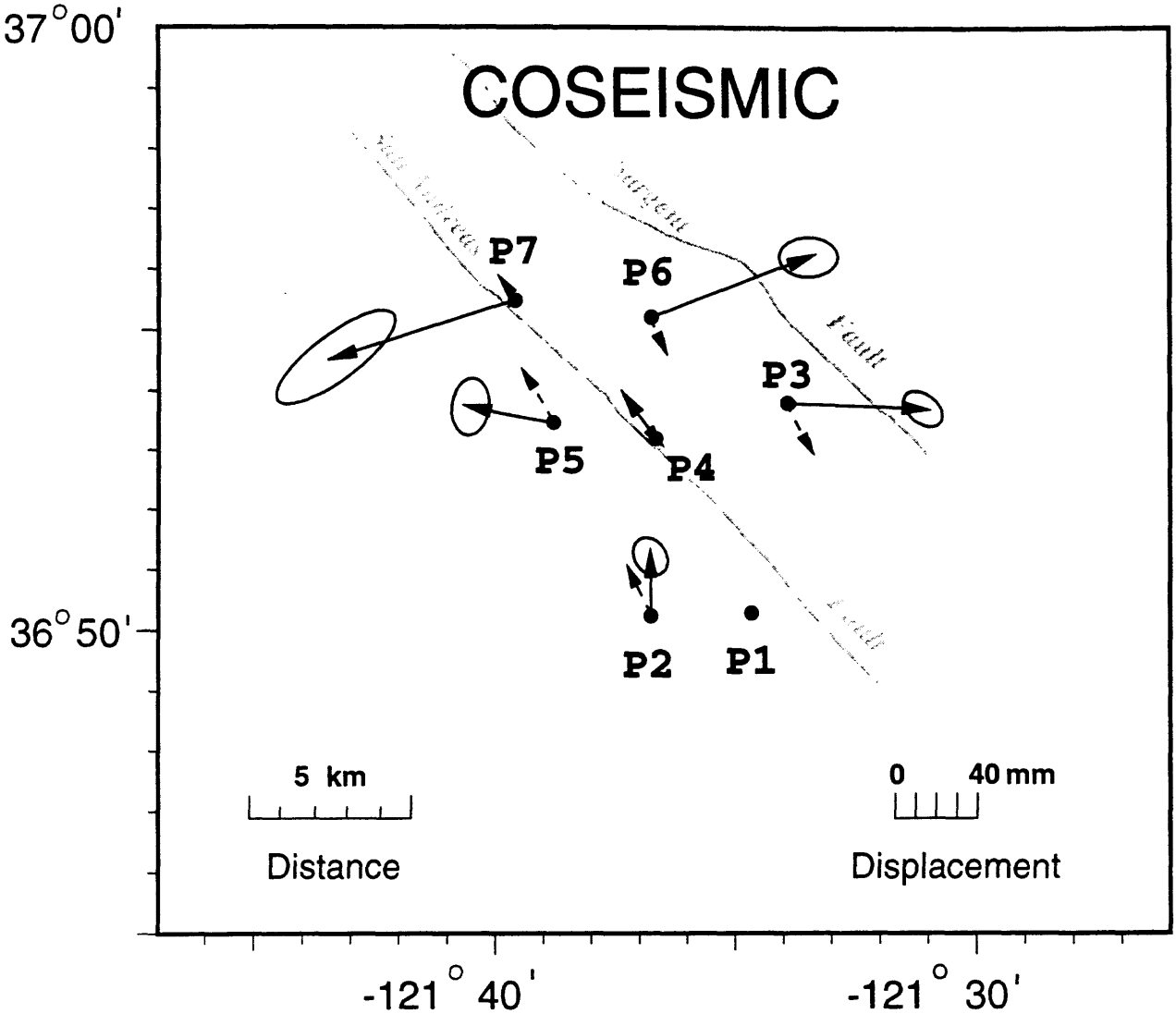

Figure 6. Observed coseismic displacement vectors obtained by a network adjustment analysis in which the position of the site P1 and the direction of the line P1-P4 are held fixed (see text). Also shown (dashed) are the vector displacements expected at each of the sites expected with the same network adjustment analysis for the AS model (see text) of the primary Loma Prieta rupture.

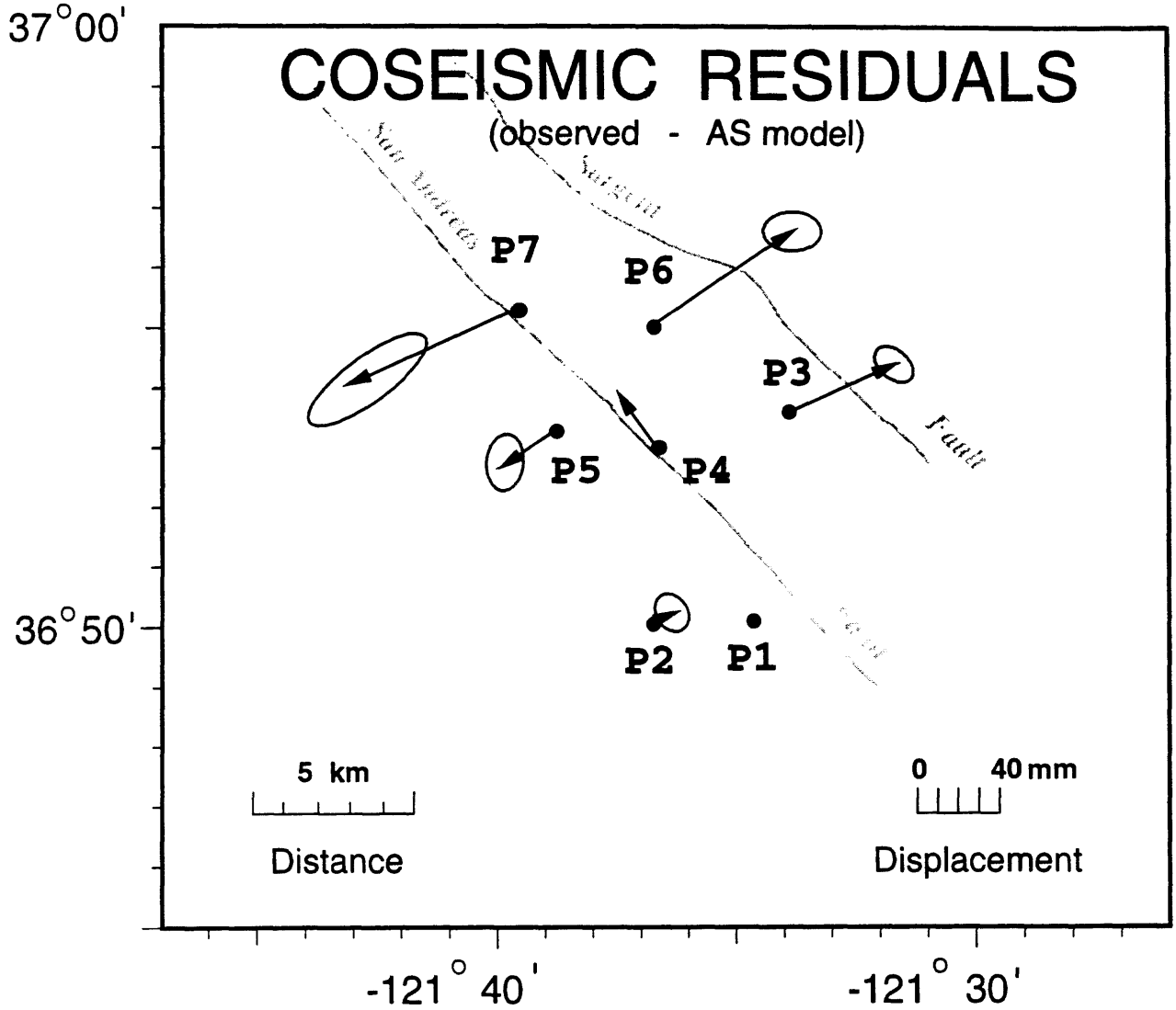

Figure 7. Residual coseismic displacement vectors (solid lines) and errors obtained when the calculated displacements for the Loma Prieta AS model are subtracted from the observations. Again, the position of the site P1 and the direction of the line P1-P4 are held fixed (see text).

cally questionable, in that, while we find we need 70 cm of strike-slip motion on an 8 km by 3 km vertical fault patch on the San Andreas fault and 80 cm of primarily strike-slip motion on an 10 km by 4 km fault patch on the Sargent fault, we also need 40 cm of extension on the San Andreas fault. While seismicity in this region (Fig. 3) does show an apparent right step between sites P4 and P5, this extension is too large to be acceptable. What this is probably trying to tell us is we need some component of thrust near the San Andreas to explain the eastward movement of sites P3 and P6. However, we do not have sufficient data to justify searching for a more general model.

More likely models, such as that listed in Table 3, were obtained if the San Andreas fault was allowed some dip (80 degrees) in this region. In this model we have 57 cm of oblique slip on an 8 km by 3 km patch of the San Andreas fault with a dip of 80 degrees and 86 cm of strike-slip on a 10 km by 4 km vertical patch on the Sargent fault. The model misfit in this case was 4.6 mm/mm and it is clear the fit is poor at sites P3 and P6. The locations of the two slip patches for this model are shown on the upper cross-section plot of the region in Figure 8 together with the maximum depth of seismicity (shown as a dashed line). Calculations of line-length changes for each of the lines obtained when this additional slip model is included with the AS model are shown in Table 2 together with the residuals when the total model calculations (AS + Table 3 Model) are subtracted from the data. Except for baselines involving sites P3 and P6, these residuals are now generally within the observational error. The total model displacement vectors (dashed) are shown in Figure 9 with the observed displacement vectors (solid) showing that the overall fit to the data is improved. The additional moment release on this segment of the San Andreas fault system was 1.4×10^{18} Nm. More complex models with additional slip patches, slightly different geometry, steeper dip or perhaps including differential slip on these patches might give a better fit to these data but with the few data we have we cannot justify invoking more parameters.

Few data exist in this region that might be used to independently test this new total Loma Prieta rupture model. It is a great relief that the coseismic data from the two borehole strainmeters SRL and SJB (Figure 1) within the network (*Johnston et al.*, 1990) are now generally consistent with this new model, as they should since these data were used to obtain this model. Previously, the observed coseismic offsets could not be reconciled with calculations based on any of the other coseismic models (*Johnston et al.*, 1990). The observed coseismic dilatational strain step at SRL is +5.0 microstrain while the dilatation, $\gamma 1$ ($=e_{xx}-e_{yy}$) shear, and $\gamma 2$ ($=2e_{xy}$) shear at SJB are +1.3, +1.8, and -3.8 microstrain, respectively (*Johnston et al.*, 1990). Using the total rupture model, the calculated dilatational strain at SRL is +3.9 microstrain, while the calculated tensor strain values at SJB are +2.0 microstrain in dilatation, +2.0 microstrain in $\gamma 1$ shear, and -5.2 microstrain for $\gamma 2$ shear.

Table 3. Best Fitting Fault Parameters for Uniform Slip Models

FAULT	STRIKE	DIP	LATITUDE	LONGITUDE	TOP	WIDTH	LENGTH	STRIKE-SLIP	DIP-SLIP	DILATATION	MOMENT
	---------- degrees ----------				km	km	km	m	m	m	10^{-18} MPa
					COSEISMIC MODEL 1						
San Andreas	N45W	90	36 54.5'	-121 38.8'	2.0	3	8	0.7	0.0	0.4	0.8
Sargent	N60W	90	36 57.9'	-121 35.7'	1.0	4	10	0.8	0.1	0.0	1.0
					COSEISMIC MODEL 2						
San Andreas	N45W	90	36 54.5'	-121 38.8'	3.0	3	8	0.35	0.45	0.0	0.4
Sargent	N60W	90	36 57.9'	-121 35.7'	1.0	4	10	0.5	-0.7	0.0	1.0
					POSTSEISMIC MODEL						
San Andreas	N45W	90	36 58.4'	-121 45.0'	2.0	10	9	0.6	0.0	0.0	1.6
San Andreas	N45W	90	36 58.1'	-121 43.8'	1.0	3	24	0.15	0.0	0.0	0.3

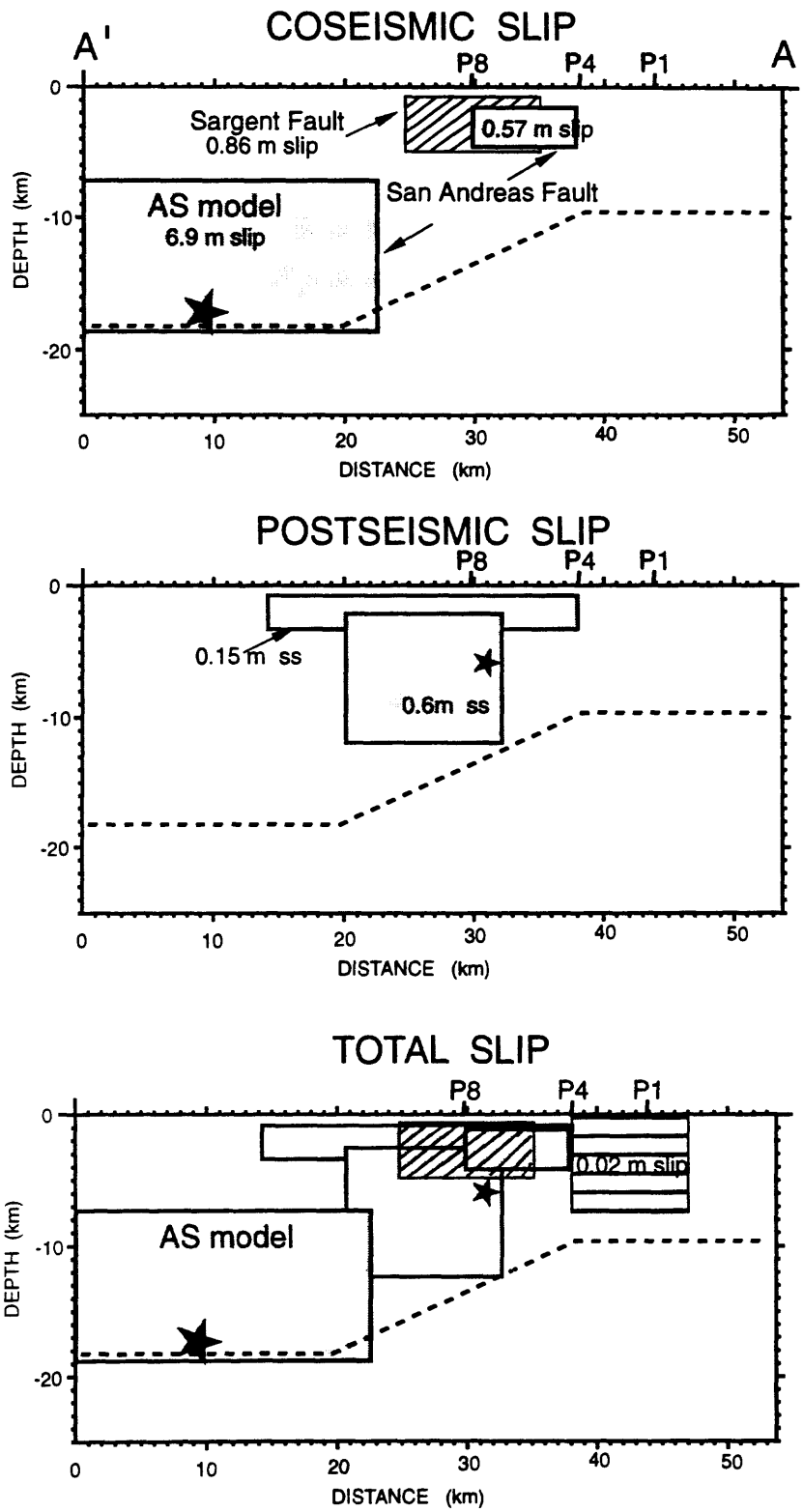

Figure 8. Fault cross-sections showing the geometry and location in relation to the Loma Prieta rupture (AS model- see text) of the best-fitting slip patches on the San Andreas and Sargent faults that generate 1) the observed coseismic displacements in the Pajaro EDM network (top plot), and 2) the observed postseismic displacements (middle plot). The bottom plot shows the location and geometry of the total slip (coseismic and postseismic) patches on the San Andreas and Sargent faults again in relation to the AS Loma Prieta model. Also shown (horizontal hatching) is the location of the slip patch proposed by Linde et al., [1996] to fit strain observed during a slow earthquake in December, 1996.

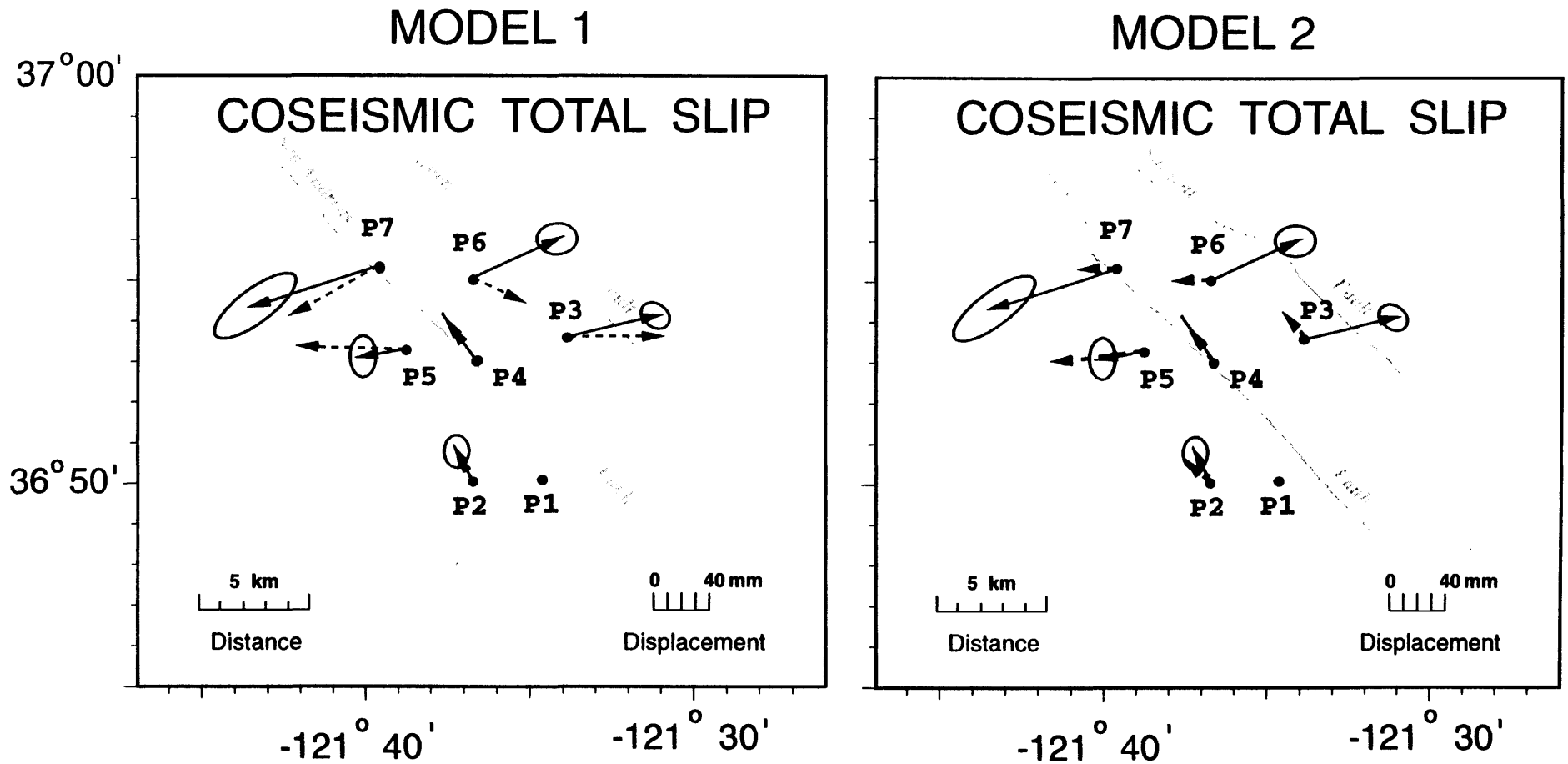

Figure 9. Observed coseismic displacement vectors (solid lines) obtained by a network adjustment analysis in which the position of the site P1 and the direction of the line P1-P4 are held fixed (see text) in relation to those expected from the total Loma Prieta slip model (dashed). Model 1 is the best fit, but requires 40 cm of extension on the San Andreas Fault (Table3). Model 2 includes only oblique slip on both the San Andreas and Sargent Faults. While model 2 fits most of the observed linelength changes, it does not fit the coseismic offsets observed on lines P5-P6 and P3-P4 (Table 2).

The values are in good agreement in sign and amplitude with those at the SJB tensor strainmeter and the dilational strainmeter SRL. This new total model, or some other like it, thus supplies a possible answer to the strain offset problem in this region pointed out by *Johnston et al.* (1990). A single level-line was run through the Pajaro Gap following the earthquake (*Marshall et al.*, 1991). Unfortunately, the data were too infrequent to separate coseismic and postseismic vertical displacements in the region. However, these data do indicate that the Loma Prieta earthquake did generate vertical displacements on the Sargent fault in support of our contention that slip occurred here during the earthquake.

The postseismic line length changes observed between 1989 and 1992 are shown in Figure 5 and are listed in Table 4. As with the coseismic phase of the earthquake, the largest postseismic displacements also occur beneath the northern part of the Pajaro net. Furthermore, the majority of these postseismic changes occur between the 1989 survey and the October 1990 survey and, during this time period, a M_L 5.4 aftershock occurred beneath the network at Chittenden on April 18, 1990.

We now investigate models of local slip that will satisfy the postseismic observations. We again restrict our search for slip models to those on the San Andreas and/or Sargent faults where aftershock activity was concentrated and solve for slip, and perturbations in length and width. The best fitting model obtained implies 60 cm and 15 cm of post-seismic strike-slip motion on two overlapping slip patches along the San Andreas fault, Table 3. No additional slip is required on the Sargent Fault. For this model, the misfit was 1.7 mm/mm. The locations of these two postseismic slip patches are shown on the middle cross-section plot of the region in Figure 8. The deeper patch is located along the fault northwest from the coseismic patch and probably represents filling in of slip between the Loma Prieta main rupture and the secondary coseismic rupture beneath the network. More importantly, this postseismic slip patch on the San Andreas includes the April 18 Chittenden earthquake (location shown as a star in the middle plot in Figure 8). Thus, it is possible that this earthquake may have either triggered post-seismic slip at this location, or the earthquake was triggered by post-seismic slip. The moment release was 1.9×10^{18} Nm or about a factor of 10 larger than that released by the Chittenden earthquake.

The model predictions for this postseismic slip and line-length changes for each of the lines obtained from this slip model are listed in Table 4 together with the residuals when the model predictions are subtracted from the observed data. These residuals are within the observational error. A comparison of observations (solid lines) and model displacement vectors (dashed lines) is shown in Figure 10. In recent papers, *Savage et al.*, (1994) and *Burgmann et al.*, (1997) have

Table 4. Summary of Postseismic Displacements (mm).

Line	Postseismic Observed	Model	Residuals (Obs. - Mod.)
	FAULT CROSSING		
P7-P8	57 ±5	57	0 ±5
P5-P7	-42 ±5	-47	5 ±5
P5-C1	-37 ±6	-40	3 ±5
P5-P6	1 ±6	16	15 ±6
P4-P5	22 ±5	26	4 ±5
P2-P4	-22 ±7	-18	4 ±7
P1-P4	-18 ± 7	-13	5 ± 7
	NONFAULT CROSSING		
P6-P7	21 ± 5	41	-20 ± 5
P4-P7	-28 ±7	-31	3 ±7
P4-P6	-22 ± 5	-9	-13 ±5
P2-P5	23 ±7	5	18 ±7
P1-P2	4 ±5	8	4 ± 5

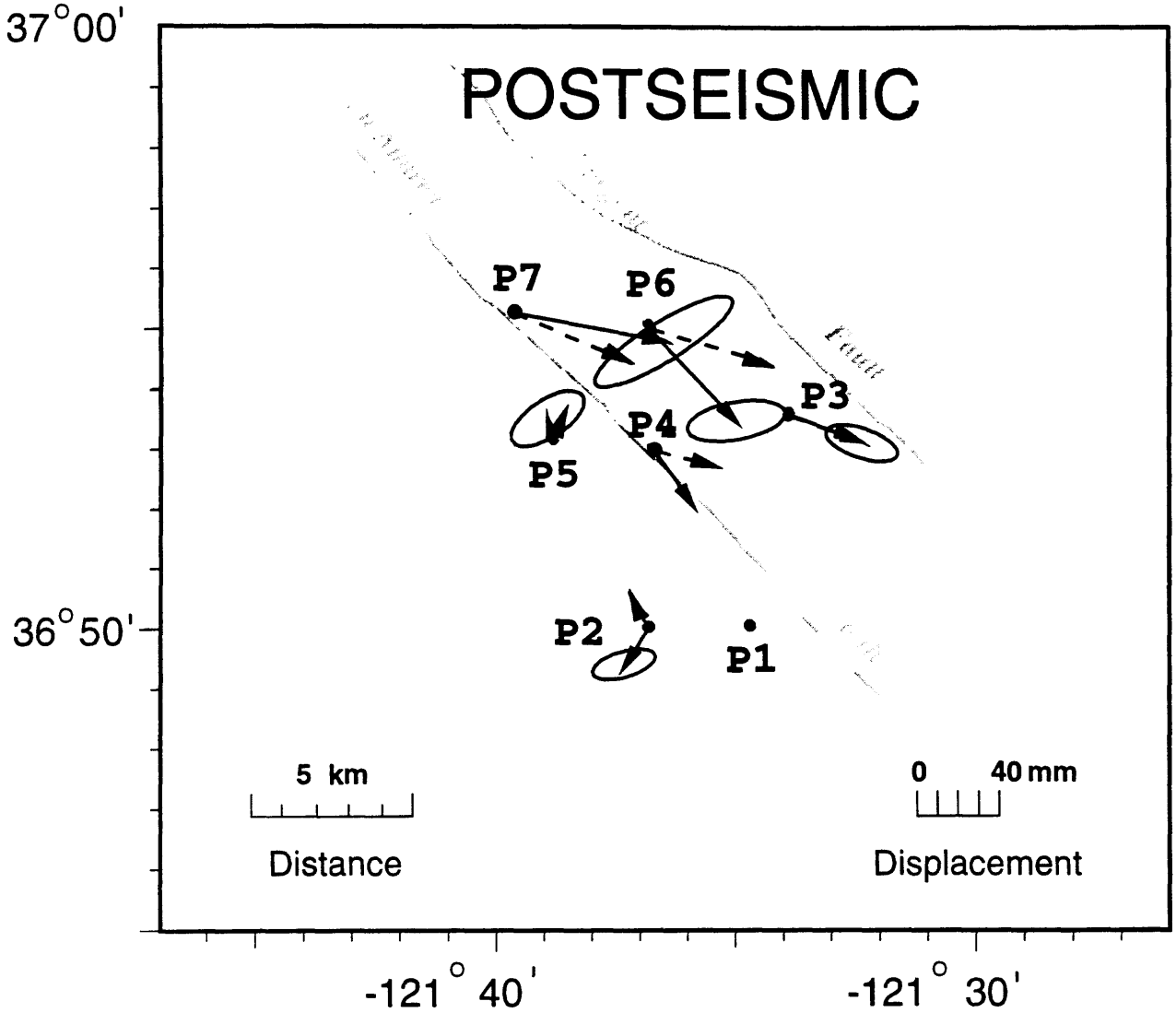

Figure 10. Observed postseismic displacement vectors obtained by a network adjustment analysis in which the position of the site P1 and the direction of the line P1-P4 are held fixed (see text) in relation to those expected from the postseismic slip model (dashed lines).

reported postseismic contraction in GPS data to the north-east of the Loma Prieta epicenter some 20 km to 30 km to the north of the Pajaro array. *Savage et al.*, (1994) suggested that fault zone compaction in the hypocentral region may explain the observed motions while *Burgmann et al.*, (1997) suggested these might have resulted from two reverse faults dipping westward from beneath the San Andreas and Sargent faults. While *Burgmann et al.*, (1997)'s reverse fault model extends through the Pajaro network, the expected displacements are not consistent with our observations and the proposed fault is at an angle of 54 degrees to the observed vertical seismicity on the Sargent fault. However, *Burgmann et al.*,'s (1997) model is very poorly constrained in this region and perhaps reverse faults that do not extend 20 km to the SE through the Pajaro network might still fit the data. Expected displacements at Burgmann et al., (1997)'s GPS sites from the model proposed here amount to several centimeters in a generally southerly direction, similar to those observed.

We do find suggestions in some lines of increases in the displacement rates of the fault crossing lines (Figure 5) following the Loma Prieta earthquake in the San Juan Bautista/Pajaro gap region of the SAF. Future data will determine whether this is the case. We suspect it to be so since higher postseismic creep rates [13.4 mm/yr at Nyland Ranch (*Behr et al.*, 1996)] and higher continuous shear-strain rates (*Gwyther et al.*, 1992) are observed in the region.

The net total slip (coseismic and postseismic) in this region is shown in the bottom cross-section plot in Figure 8. An interesting feature of this plot is that almost all of the 15 km long segment of the San Andreas north of site P4 and down to the bottom of the microseismicity appears to have slipped during and following the Loma Prieta earthquake. Another interesting feature of the plot is that the segment of the fault south of P4 slipped in slow earthquakes in 1992 and 1996 (*Linde et al.*, 1996; *Johnston et al.*, 1997). The model used to fit the 1992 strain data (*Linde et al.*, 1996) is shown as a cross-hatched section on the bottom plot of Figure 8. Substantial slip moment (2.7×10^{18} Nm) has thus been released on this segment of the San Andreas fault as a consequence of the Loma Prieta earthquake.

Conclusions

Ground displacements measured on an intermediate baseline geodetic network spanning 14 km of the San Andreas from San Juan Bautista to Pajaro Gap are not consistent with rupture models of the Loma Prieta earthquake derived from inversions of geodetic and strong motion data. Additional slip is required on both the San Andreas and the Sargent faults near this network. Model fits to

these data indicate substantial coseismic slip occurred on the San Andreas fault beneath this network with sympathetic slip on the nearby Sargent fault during the Loma Prieta earthquake though we have too few data to provide tight constraints on these models. The total moment release was 4×10^{17} Nm on the San Andreas and 1.0×10^{18} Nm on the Sargent fault and increases by 5% the total moment release for the Loma Prieta earthquake reported by *Lisowski et al.* (1990) and *Arnadottir and Segall* (1994). Coseismic strain steps calculated at borehole strainmeter sites within the Pajaro network by a Loma Prieta model that includes this additional moment release at the southern end of the Loma Prieta primary rupture are now in good agreement with strain observations from these sites.

Time varying postseismic displacements occurred on the San Andreas fault mostly during the year following the Loma Prieta earthquake. These displacements are consistent with postseismic slip on the San Andreas fault beneath the network. The moment release of 1.9×10^{18} Nm appears concentrated in the region beneath the north part of the network where a magnitude 5.4 earthquake occurred on April 18, 1990. This event was apparently triggered by the slip or played a role in triggering the slip.

Finally, future data from these sites will confirm whether the Loma Prieta earthquake increased the block slip rate in the Pajaro region. The slip rate is well determined by *Gu and Prescott* (1986) *Lisowski et al.*, (1996) and *Behr et al.*, (1997) prior to the Loma Prieta earthquake. Following the event, higher creep rates (*Behr et al.*, 1996), higher continuous shear-strain rates (*Gwyther et al.*, 1992) and several aseismic slip events (slow earthquakes) have been observed in the region. Will a damaging earthquake occur in this region in the near future? On one hand, the Loma Prieta earthquake certainly increased shear stress on the fault and thus increased the likelyhood of a damaging earthquake, as suggested by *Behr et al.* (1997). On the other hand, considerable slip moment has been released in the region and most of the fault has failed in some form since the Loma Prieta earthquake. It thus seems unlikely that such a weakened fault could support a significant earthquake in the near future along this segment of the San Andreas fault.

Acknowledgements

We thank Glen Deardorf, Conrad Van Bruggen, Amy Rapport, Stan Silverman, Doug Myren, Vince Keller, Bob Bielinski and others for their perseverance in obtaining the observations and Karen Wendt for help in processing the data. We also thank Roland Burgmann and an unidentified

reviewer for useful review comments.

References

Arnadottir, T., and P. Segall, The 1989 Loma Prieta earthquake imaged from inversion of geodetic data, *J. Geophys. Res.*, **99**, 21,835-21,855, 1994.

Aydin A., A. M. Johnson, and R. W. Fleming, Right-lateral-reverse surface rupture along the San Andreas and Sargent faults associated with the October 17, 1989, Loma Prieta, California earthquake, *Geology*, **20**, 1063-1067, 1992.

Beroza, G. C., Near-source modeling of the Loma Prieta earthquake: Evidence for heterogeneous slip and implications for earthquake hazard, *Bull. Seis. Soc. Am.*, **81**, 1603-1621, 1991.

Bevington, P. R., Data reduction and error analysis for the physical sciences, 336 pp., McGraw-Hill, New York, 1969.

Behr, J., R. Bilham, and P. Bodin, Increased surface creep rates on the San Andreas fault southeast of Loma Prieta mainshock, *U.S. Geol. Surv. Prof. Pap.*, **1550-D**, 179-192, 1997.

Bomford, G., Geodesy, Oxford University Press, London, 1971.

Burgmann, R., P. Segall, and J. Svarc, Postseismic strain following the 1989 Loma Prieta earthquake from GPS and leveling measurements, *J. Geophys. Res.*, **102**, 4933-4956, 1997.

Dietz, L., and W. L. Ellsworth, The October 17, 1989, Loma Prieta earthquake and its aftershocks: Geometry of the sequence for high-resolution locations, *Geophys. Res. Lett.*, **17**, 1417-1420, 1990.

Gu, G. and W. H. Prescott, Discussion on displacement analysis: Detection of crustal deformation, *J. Geophys. Res.*, **91**, 7439-7446, 1986.

Gwyther, R. L., M. T. Gladwin, and R. H. G. Hart, A shear strain anomaly following the Loma Prieta earthquake, *Nature*, **356**, 142-144, 1992.

Hartzell, S. H., G. S. Stewart, and C. Mendoza, Comparison of L_1 and L_2 norms in a teleseismic waveform inversion for the slip history of the Loma Prieta, California, earthquake, *Bull. Seis. Soc. Am.*, **81**, 1518-1539, 1991.

Horton, S., A fault model with variable slip duration for the 1989 Loma Prieta, California, earthquake determined from strong-ground-motion data, *Bull. Seis. Soc. Am.*, **86**, 122-132, 1996.

Johnston, M. J. S., A. T. Linde, and M. T. Gladwin, Near-field high precision strain prior to the October 18, 1989 Loma Prieta M_L 7.1 earthquake. *Geophys. Res Lett.*, **17**, 1777-1780, 1990.

Johnston, M. J. S., R. Gwyther, R. J. Mueller, A. T. Linde, M. T. Gladwin, and G. D. Myren, Another slow earthquake on the San Andreas fault triggered by a M4.7 earthquake on April 19, 1996. *Trans. Am. Geophys. Un.*, **78**, S209, 1997.

Linde, A. T., M. T. Gladwin, M. J. S. Johnston, R. L. Gwyther, and R. Bilham, A slow earthquake near San Juan Bautista, California, in December, 1992, *Nature.*, **383**, 65-68, 1996.

Lisowski, M., and W. H. Prescott, Short-range distance measurements along the San Andreas fault system in central California, 1975 to 1979, *Bull. Seis. Soc. Am..*, **71**, 1607-1624, 1981.

Lisowski, M., M. H. Murray, and J. Svarc, Geodetic Measurements of coseismic horizontal deformation, *U.S. Geol. Surv. Prof. Pap.*, **1550A**, 81-103, 1996.

Lisowski, M., W. H. Prescott, M. J. Johnston, and J. C. Savage, Geodetic estimate of coseismic slip during the 1989 Loma Prieta, California, earthquake, *Geophys. Res. Lett.*, **17**, 1437-1440, 1990.

Marquardt, D. W., An algorithm for least-squares estimation of nonlinear parameters, *J. Soc. Ind. Appl. Math.*, **11**, 431-441, 1963.

Marshall, G. A., R. S. Stein, and W. Thatcher, Faulting geometry and slip from co-seismic elevation changes: The October 18, 1989, Loma Prieta California earthquake, *Bull. Seis. Soc. Am.*, **81**, 1660-1693, 1991.

Okada, Y., Surface deformation due to shear and tensile faults in a half-space, *Bull. Seis. Soc. Am.*, **75**, 1135-1154, 1985.

Prescott, W. H., The determination of displacement fields from Geodetic data along a strike-slip fault, *J. Geophys. Res.*, **86**, 6067-6072, 1981.

Savage, J. C. and W. H. Prescott, Precision of Geodolite distance measurements for determining fault movements, *J. Geophys. Res.*, **78**, 6001-6008, 1973.

Savage, J. C., M. Lisowski, and J. L. Svarc, Postseismic deformation following the 1989 (M = 7.1) Loma Prieta, California, earthquake, *J. Geophys. Res.*, **99**, 13,757-13,765, 1994.

Snay, R. A., H. C. Neugebauer, and W. H. Prescott, Horizontal deformation associated with the Loma Prieta earthquake, *Bull. Seis. Soc. Am.*, **81**, 1647-1659, 1991.

Steidl, J. H., R. J. Archuleta, and S. H. Hartzell, Rupture history of the 1989 Loma Prieta, California, earthquake, *Bull. Seis. Soc. Am.*, **81**, 1573-1602, 1991.

Wald, D. J., D. V. Helmburger, and T. H. Heaton, Rupture model of the 1989 Loma Prieta earthquake from inversion of strong-motion and broad-band teleseismic data, *Bull. Seis. Soc. Am.*,

81, 1540-1572, 1991.

Wesson, R. L., R. O. Burford, and W. L. Ellsworth, Relationship between seismicity fault creep and crustal loading along the central San Andreas fault, *Proc. Conf. Tect. Prob. San Andreas Fault System*, Stanford University Publication Geological Sciences, **Vol XIII**, 303-321, 1973.

Williams, C. R., T. Arnadottir, and P. Segall, Coseismic deformation and dislocation models of the 1989 Loma Prieta earthquake derived from Global Positioning System measurements, *J. Geophys. Res.*, **98**, 4567-4578, 1993.

Welsch, W., A review of the adjustment of free networks, *Surv. Rep. Gt. Brit.*, **25(194)**, 167-180, 1979.

R. Mueller, U. S. Geol. Surv., ms/977, 345 Middlefield Rd., Menlo Park, CA 94025. (e-mail: rmueller@usgs.gov)

M. J. S. Johnston, U. S. Geol. Surv., ms/977, 345 Middlefield Rd., Menlo Park, CA 94025. (e-mail: mal@usgs.gov)

APPENDIX A

PAJARO NETWORK HP LASER RANGING MEASUREMENTS

FAULT CROSSING LINES

DATE	LINE	MARK-MARK DISTANCE	FLAT-EARTH DISTANCE	SIGNAL STRENGTH
		P1-P3		
090981	p1-p3	6579.105	6576.034	64-65
091481	p3-p1	6579.109	6576.038	59-61
061582	p1-p3	6579.118	6576.047	43-52
070882	p3-p1	6579.110	6576.039	56-63
061082	p3-p1	6579.102	6576.030	51-56
121289	p3-p1	6579.098	6576.027	51-52
102690	p1-p3	6579.073	6576.002	70
103090	p3-p1	6579.079	6576.008	50-58
		"lost benchmark"		
		P1-P4		
083181	p1-p4	6634.285	6633.916	52-55
090181	p4-p1	6634.314	6633.944	47-51
071082	p4-p1	6634.294	6633.925	51-60
071082	p4-p1	6634.288	6633.918	47-60
102789	p4-p1	6634.280	6633.911	60-63
121289	p1-p4	6634.260	6633.891	50
112089	p4-p1	6634.282	6633.913	54-60
102690	p1-p4	6634.259	6633.890	50
102690	p4-p1	6634.258	6633.889	61-64
061991	p4-p1	6634.250	6633.881	61-69
051992	p1-p4	6634.262	6633.892	61-71
051492	p4-p1	6634.252	6633.882	55-69
091196	p1-p4	6634.213	6633.843	59-74
091196	p4-p1	6634.213	6633.843	64-75
		P2-P4		
090281	p2-p4	5392.855	5391.497	61-62
090181	p4-p2	5392.846	5391.489	57-59
071082	p2-p4	5392.843	5391.486	57-66
071582	p2-p4	5392.843	5391.486	59-61
112089	p4-p2	5392.829	5391.472	66-71
121489	p2-p4	5392.818	5391.461	50-60
102690	p4-p2	5392.813	5391.455	62-65
061991	p4-p2	5392.811	5391.454	58-74
051492	p4-p2	5392.805	5391.447	72-76
051992	p2-p4	5392.801	5391.443	71-79
		P4-P5		
081381	p4-p5	3240.362	3240.354	69-76
081881	p5-p4	3240.360	3240.353	73-74
082282	p4-p5	3240.365	3240.357	70-74
062282	p5-p4	3240.361	3240.354	62-66
102789	p4-p5	3240.420	3240.412	71-73
102789	p5-p4	3240.410	3240.403	68-70
102690	p4-p5	3240.414	3240.406	71-73
102690	p5-p4	3240.417	3240.410	73-75
051492	p4-p5	3240.436	3240.428	57-67
051992	p5-p4	3240.441	3240.434	59-73

NON-FAULT CROSSING LINES

DATE	LINE	MARK-MARK DISTANCE	FLAT-EARTH DISTANCE	SIGNAL STRENGTH
		P1-P2		
083181	p1-p2	4002.836	3998.276	72-73
090281	p2-p1	4002.844	3998.284	69
070882	p1-p2	4002.837	3998.277	53-60
071082	p2-p1	4002.841	3998.281	64-72
112289	p2-p1	4002.839	3998.280	48-52
121289	p1-p2	4002.854	3998.294	62-69
102690	p1-p2	4002.860	3998.301	68-70
103090	p2-p1	4002.867	3998.307	51-70
051892	p1-p2	4002.854	3998.295	74-80
051992	p2-p1	4002.845	3998.286	69-80
		P2-P5		
082181	p2-p5	6597.597	6596.355	51-60
081881	p5-p2	6597.584	6596.342	40-55
071082	p2-p5	6597.580	6596.339	44-56
071582	p2-p5	6597.574	6596.332	44-53
121489	p2-p5	6597.565	6596.323	50-60
103090	p2-p5	6597.570	6596.328	56-65
102690	p5-p2	6597.594	6596.352	51-60
051992	p2-p5	6597.579	6596.337	55-76
051992	p5-p2	6597.595	6596.354	60-78
		P3-P4		
091781	p3-p4	4291.934	4289.935	74-78
090381	p4-p3	4291.932	4289.932	50-54
070882	p3-p4	4291.939	4289.939	61-68
061182	p4-p3	4291.936	4289.936	52
121289	p3-p4	4292.010	4290.011	70
112089	p4-p3	4292.013	4290.013	63-65
103090	p3-p4	4292.021	4290.021	58-66
102690	p4-p3	4292.020	4290.020	63-70
061991	p3-p4	4292.018	4290.019	48-55
061991	p4-p3	4292.020	4290.023	69-81
		"lost benchmark"		
		P3-P6		
091481	p3-p6	5040.350	5039.436	63-64
082681	p6-p3	5040.348	5039.434	75
061082	p3-p6	5040.353	5039.438	50-58
061182	p6-p3	5040.354	5039.439	60
121289	p3-p6	5040.361	5039.447	62-64
112089	p6-p3	5040.356	5039.442	48-57
103090	p3-p6	5040.341	5039.427	48-63
103090	p6-p3	5040.339	5039.425	48-65
		"lost benchmark"		
		P4-P6		
090181	p4-p6	3745.047	3744.884	70-73
082781	p6-p4	3745.042	3744.878	75-77
062282	p4-p6	3745.037	3744.873	62-66

091196 p4-p5 3240.474 3240.466 65-71
091196 p5-p4 3240.466 3240.459 50-72

P5-P6

081881 p5-p6 4449.844 4449.646 55-70
082781 p6-p5 4449.836 4449.638 74
070782 p5-p6 4449.845 4449.647 46-52
070782 p6-p5 4449.850 4449.651 60-75
102789 p5-p6 4449.935 4449.737 62-71
112089 p6-p5 4449.926 4449.728 63-67
102690 p5-p6 4449.922 4449.723 62-65
102690 p6-p5 4449.932 4449.734 49-66
051992 p5-p6 4449.933 4449.735 65-75
051992 p6-p5 4449.931 4449.733 67-75
091196 p5-p6 4449.918 4449.720 63-79
091296 p6-p5 4449.922 4449.724 72-78

P5-C1

092281 p5-c1 5514.170 5510.964 70-71
092281 c1-p5 5514.179 5510.973 64-68
072182 p5-c1 5514.190 5510.984 51-66
072182 p5-c1 5514.187 5510.981 52-69
102789 p5-c1 5514.151 5510.945 51-54
112189 c1-p5 5514.127 5510.921 58-66
102990 c1-p5 5514.108 5510.903 52-66
102990 p5-c1 5514.105 5510.899 65-70
051892 c1-p5 5514.090 5510.884 60-74

P5-P7

091381 p7-p5 4128.312 4121.900 67-70
072182 p5-p7 4128.307 4121.895 49-50
072282 p7-p5 4128.309 4121.897 61-71
072282 p7-p5 4128.308 4121.896 59-68
112189 p7-p5 4128.262 4121.850 63-69
112189 p7-p5 4128.256 4121.844 63-68
102990 p5-p7 4128.226 4121.814 70
102990 p7-p5 4128.215 4121.802 66-71
051892 p7-p5 4128.211 4121.799 60-80
051892 p7-p5 4128.222 4121.810 69-78
091096 p7-p5 4128.179 4121.767 57-62

P7-P8

072282 p7-p8 2973.169 2960.884 60-74
072282 p7-p8 2973.168 2960.883 60-73
112189 p7-p8 2973.247 2960.962 64-75
112189 p7-p8 2973.250 2960.966 56-72
102990 p7-p8 2973.303 2961.019 59-65
102990 p8-p7 2973.294 2961.010 70
051892 p7-p8 2973.311 2961.026 71-80
051892 p7-p8 2973.300 2961.016 74-78
091096 p7-p8 2973.326 2961.042 58-78

070782 p6-p4 3745.035 3744.871 71-75
112089 p4-p6 3745.036 3744.872 54-62
112089 p6-p4 3745.047 3744.884 55-74
102690 p6-p4 3745.033 3744.869 59-70
069191 p4-p6 3745.025 3744.861 70-85
061991 p6-p4 3745.022 3744.859 67-69
051492 p4-p6 3745.018 3744.854 72-77
051992 p6-p4 3745.022 3744.858 72-78
091196 p4-p6 3744.999 3744.836 76-80
091296 p6-p4 3745.004 3744.841 59-79

P4-P7

081781 p4-p7 6288.369 6284.413 52-72
091381 p7-p4 6288.375 6284.420 49-54
072282 p7-p4 6288.377 6284.422 48-62
072282 p7-p4 6288.380 6284.424 48-61
112189 p7-p4 6288.395 6284.439 45-57
102690 p4-p7 6288.342 6284.387 56-65
102990 p7-p4 6288.354 6284.399 46-61
051892 p7-p4 6288.364 8284.408 59-70
051892 p7-p4 6288.362 6284.407 60-72
091096 p7-p4 6288.395 6284.440 65-73

P6-P7

112189 p7-p6 4369.677 4365.631 58-71
112189 p7-p6 4369.664 4365.618 58-68
102990 p7-p6 4369.684 4365.638 46-63
102990 p6-p7 4369.661 4365.615 70
051892 p7-p6 4369.689 4365.643 60-70
051892 p7-p6 4369.695 4365.649 65-78
091096 p7-p6 4369.701 4365.655 58-67

APPENDIX B

BENCHMARK LOCATIONS, ELEVATIONS, AND LINE AZIMUTH

Site	Latitude	Longitude
P1PM	36° 50.33′	-121° 34.74′
	36.8389°	-121.5429°
P2PM	36° 50.31′	-121° 36.84′
	36.8386°	-121.5862°
P3PM	36° 53.83′	-121° 33.92′
	36.8973°	-121.5375°
P4PM	36° 53.25′	-121° 36.72′
	36.8875°	-121.5843°
P5PM	36° 53.52′	-121° 38.87′
	36.8920°	-121.6200°
P6PM	36° 55.26′	-121° 36.81′
	36.9211°	-121.5858°
P7PM	36° 55.54′	-121° 39.68′
	36.9258°	-121.6336°
P8PM	36° 55.78′	-121° 41.64′
	36.9298°	-121.6663°
C1PM	36° 56.08′	-121° 39.02′
	36.9346°	-121.6503°

Line	azimuth	elevation	
		Site 1	Site 2
P1-P2	271°	144 m	335 m
P1-P3	004°	144 m	345 m
P1-P4	326°	144 m	214 m
P2-P4	002°	335 m	214 m
P2-P5	331°	335 m	207 m
P3-P4	255°	345 m	214 m
P3-P6	302°	345 m	249 m
P4-P5	279°	214 m	207 m
P4-P6	179°	214 m	249 m
P4-P7	315°	214 m	437 m
P5-P6	044°	207 m	249 m
P5-P7	163°	207 m	437 m
P5-C1	331°	207 m	395 m
P6-P7	279°	249 m	437 m
P7-P8	278°	437 m	167 m